Journal of Membrane Science and Research 5 (2019) 295-302

Journal of Membrane Science & Research

journal homepage: www.msrjournal.com

Research Paper

Modeling and Simulation of CO_2 Absorption Enhancement in Hollow-Fiber Membrane Contactors using CNT–Water-Based Nanofluids

Nayef Ghasem *

Department of Chemical & Petroleum Engineering, UAE University, Alain City, UAE

Article info

Received 2018-12-23
Revised 2019-05-15
Accepted 2019-05-19
Available online 2019-05-19

Keywords

Membrane contactor
Hollow fiber
Nanofluid
CO_2 absorption
Modeling and simulation
CFD

Graphical abstract

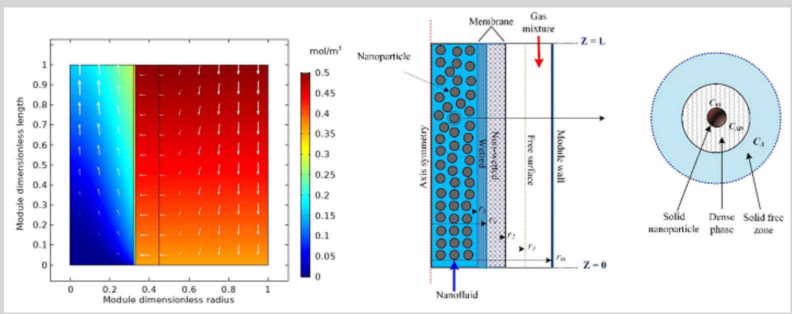

Highlights

- Modeling of the CO_2 absorption with nanofluids in membrane contactor
- Influence of the wetting in the modeling of nanofluids was considered.
- Results of the modelling were improved by assuming partial wetting mode.
- Modeling predictions were in good agreement with experimental data.

Abstract

Absorption of CO_2 from a gas mixture containing CO_2 and nitrogen by water-based CNT nanofluids in gas–liquid hollow fiber membrane contactor was modeled and solved using COMSOL Multiphysics 5.4. The model assumed partial wetting of the membrane, along with diffusion in the axial and radial directions. In addition, Brownian motion and grazing effects were both considered in the model. The main contribution to the mass transfer resistance for the case of external diffusion-controlled adsorption is the stagnant liquid layer around the particles, despite the layer being very thin. Accordingly, the nanofluid flows in the lumen tube side of the hollow fiber membrane was modeled as a solid-free zone and dense solid phase. The simulations were performed using 7% wetting of the membrane thickness. The results showed a significant increase in CO_2 absorption with increasing concentration of carbon nanotubes (CNT). At a fixed inlet gas flow rate (20 L/h), increasing the CNT concentration from 0.1 wt.% to 0.25 wt.% increased the CO_2 removal from around 20% to 45%. Comparison of the model predictions with experimental data available in the literature confirmed the validity of the developed model.

1. Introduction

Huge amounts of carbon dioxide (CO_2) are being emitted into the atmosphere due to the increase in fossil fuel consumption, the majority of which release carbon dioxide [1]. The carbon dioxide and other pollutants released into the atmosphere act like as blanket, trapping the sun's heat and causing the planet to warm. The resulting weather patterns are making wet areas become wetter and dry areas become drier [2]. Natural gas is generally considered as a cleaner fuel than other fossil fuels, although it contains undesirable compounds such as CO_2 and H_2S. These impurities must be removed to meet the pipeline quality standards and consumer fuel specifications to avoid corrosion of the pipelines and equipment and enhance the calorific value of the natural gas. The presence of these impurities affects the heating value and the gas can freeze in the pipeline during the cryogenic liquefaction process used to produce liquid natural gas [3].

Absorption processes, such as packed bed or tray columns, are currently used to remove acidic gases from natural gas and flue gas. However, despite the great advantages of conventional gas–liquid absorption columns, these systems have drawbacks including channeling, entrainment, frothing, and liquid overflow [4,5]. Gas–liquid hollow fiber membrane contactors are a promising and efficient technology for removing CO_2 from gas mixtures. The separation process has been extensively investigated and the process has been recommended by many researchers [6-13]. In these systems, the membrane module is comprised of bunches of hollow fiber membranes surrounded by an external metal casing (referred to here as the shell). Usually, the liquid solvent flows through a central distribution tube inside the membrane bundle, while the gas mixture enters from the casing side. However, vice versa is also possible. The large membrane surface area per unit volume is the main advantage of the membrane contactor compared to traditional contacting columns [14-19].

Nanofluids have been used to increase the rate of absorption of the solute gas in membrane contactors. These fluids contain nanoparticle materials such as carbon nanotubes (CNT), SiO_2, Al_2O_3, and Fe_3O_4 in a base fluid, such as distilled or deionized water or amine solutions [20,21]. A schematic diagram

* Corresponding author at: Phone: +971-3-713-5313; fax: +971-3-713-4996
E-mail address: nayef@uaeu.ac.ae (N. Ghasem)

DOI: 10.22079/jmsr.2019.100177.1239

of a gas–liquid hollow fiber membrane contactor with a nanofluid flowing through the lumen tube side of the hollow fiber membranes is shown in Figure 1. In this case, a CO_2/N_2 gas mixture flows in the shell side of the membrane module.

The absorption of CO_2 in the presence of solid nanoparticles (SiO_2, Al_2O_3, CNT, and Fe_3O_4) in water and amine solutions has been experimentally investigated in a batch process to study the influence of the nanofluids on the enhancement of the absorption of carbon dioxide from gas mixtures [22]. They showed that Fe_3O_4 and CNT nanoparticles showed better CO_2 absorption at lower concentrations, while SiO_2 and Al_2O_3 nanoparticles had better performance at higher concentrations. Simultaneous absorption of CO_2 and H_2S in water using SiO_2 and expandable graphite oxide nanoparticles was experimentally investigated in a bubble column by Esmaeili et al. [23]. They found that synthetic silica nanofluid absorbed both H_2S and CO_2 better than the base fluid owing to hydrogen bonding between the gas molecules and silica groups. A significant increase in the CO_2 removal fraction using Al_2O_3 or SiO_2 nanoparticles in methanol solvent in a bubble type absorber was demonstrated [24]. Absorption of CO_2 from CO_2/air gas mixtures using aqueous nanofluids in a microporous polypropylene membrane module was experimentally investigated [25-30], where a CNT nanofluid showed better separation than a silica nanofluid. The removal fraction of the CNT nanofluid was nearly constant and increased with increasing CO_2 concentration, while that of the silica nanofluid decreased slightly with increasing CO_2 concentration due to saturation. CO_2 removal from N_2 by metal oxide nanofluids in a hollow fiber membrane contactor was experimentally investigated [31], where an aqueous 0.2 wt.% Al_2O_3 nanofluid achieved the maximum CO_2 removal rate. The effect of nanoparticle size of aqueous silica-based nanofluids on CO_2 absorption was investigated, where mass transfer was enhanced with increasing silica particle size [32].

In addition to experimental studies, numerous models have been developed to investigate hollow fiber membrane systems. Modeling of CO_2 and H_2S capture using aqueous monoethanolamine solvent was demonstrated previously as a function of CO_2 concentration across the membrane module [18]. The modeling was performed for gas flows in hollow fiber membranes operated under non-wetted or partially wetted conditions. The absorption of oxygen in the presence of nanoparticles was studied by Nagy et al. [21]. Mathematical models for both homogeneous and heterogeneous modes were developed and analyzed. The absorption rate in the presence of nanosized droplets was measured, and the enhancement of the mass transfer rate was analyzed.

Experimental data were compared to the predicted ones. Mathematical models have been developed to study CO_2 absorption in the presence of nanofluids. For example, experimental and theoretical studies were performed using nano-Al_2O_3 and CNTs in a stirred thermostatic reactor [27]. They found that Brownian motion caused micro-convection and should be considered in the analysis. Their theoretical model considered the absorption enhancement provided by the nanoparticles. Koronaki et al. developed a numerical approach to study the enhancement of CO_2 absorption using CNTs in a batch vessel [28] and observed an increase in absorption over time until an equilibrium point was reached, which is commonly observed for batch systems. Darabi et al. [29] developed a 2D mathematical model to simulate the absorption of CO_2 enhanced by a CNT nanofluid in a hollow fiber membrane contactor under non-wetted conditions. The model considers the fluid flow in the tube side as a highly dilute system; hence, the fluid flow in the lumen side of the fiber is considered a single zone and described by one continuity equation. In this case, the micro-convection effect is not considered as the flow field around the nanoparticles interacts, enhancing diffusion of the absorbed solute. In addition, the enhanced CO_2 absorption by CNT and SiO_2 nanoparticles in distilled water was mathematically modeled and the influence of certain operating parameters on the CO_2 removal rate was studied [30]. The model was developed considering radial and axial diffusion under non-wetting conditions. None of the previous models discussed here considered partial wetting of the membrane.

In the present work, a 2D mathematical model was developed to elucidate the process of enhanced absorption of CO_2 from CO_2/N_2 gas mixtures in the presence of aqueous nanofluids in a hollow fiber membrane contactor under partial wetting of the membrane. Because the resistance to flow is mainly due to the stagnant layer of liquid around the solid nanoparticles, the model divides the membrane contactor module into five segments, two in the tube side (dense and solid free-phase), membrane (wetted zone and dry zone), and shell-side gas-phase region. The influence of the nanoparticle motion is considered in the dense phase of the tube side. Partial wetting of the membrane skin is assumed in the model. Polypropylene hollow fiber membranes wet using various absorbents (deionized water, monoethanolamine (MEA), and methyldiethanolamine (MDEA)) were experimentally investigated by Lv et al. [33]. They observed an increase in mass transfer resistance and a deterioration in CO_2 absorption performance during the membrane gas absorption process for all absorbents. Hence, the equations in the present model considered membrane wetting. The governing equations were solved numerically using the finite element method with COMSOL Multiphysics version 5.4 software. The model predictions were validated by comparison with experimental data reported in the literature. In addition, the effects of the physical characteristics of the nanoparticles and operating parameters of the system on the membrane performance were investigated.

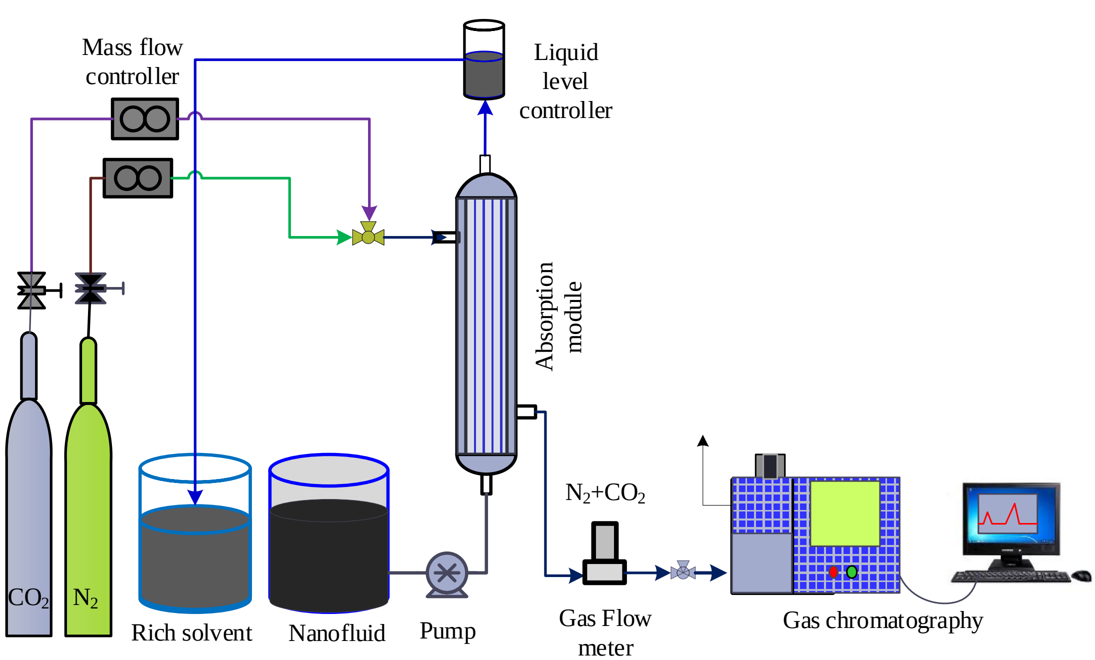

Fig. 1. Schematic diagram of an experimental setup for evaluating CO_2 absorption by a nanofluid solvent in a gas–liquid hollow fiber membrane contactor system.

2. Mathematical model

The mathematical model describes the bunch of hollow fiber membranes packed in the membrane module. Modeling of the membrane contactor module considering a cylindrical coordinate system resulted in a set of partial differential and algebraic equations that defined the material balance of the physical absorption of CO_2 using a nanofluid solvent composed of distilled water and CNTs. The membrane contactor consisted of three parts: tube, membrane, and shell section. The tube side where the nanofluid flows is modeled as a solid-free zone and dense phase. The membrane section is divided into wetted and non-wetted segments. The CO_2/N_2 gas mixture flows outside the hollow fiber membranes, while the nanofluids flow through the lumen of the hollow fiber membrane tubes in a counter-current manner, as described in Figure 2. The CO_2/N_2 gas mixture enters the membrane module from the top side (at $z = L$), while the nanofluids enter the lumen of the hollow fibers from the bottom side (at $z = 0$) in the case of vertical operation of the membrane module. Carbon dioxide diffuses from the gas mixture through the membrane pores to the nanofluid. The ability of N_2 to dissolve in an aqueous solvent is insignificant compared to that of CO_2. Hence, some of the CO_2 dissolved in the nanofluid is adsorbed on the solid nanoparticles. The CO_2 removal rate depends on the morphology of the polymeric membrane, distribution factor of CO_2, type of aqueous solvent, absorbent and nanoparticle concentrations, liquid and gas flow rates, and operating conditions.

The material balance equations used in the model describe the two main mechanisms in the presence of the nanofluid, which are Brownian motion and the grazing effect. Brownian motion of nanoparticle leads to an increase in velocity around the nanoparticle, resulting in micro-convection and the enhanced mass diffusion flux, which modifies the diffusion coefficient [27]. The grazing effect describes the adsorption of gas in the presence of nanoparticles at the gas–liquid interface [29]. The geometric variables used to develop the partial differential material balance equations in the model are shown in Figure 2. The nanofluid velocity in the tube side is assumed to be fully developed neglecting end effects and the influence of the nanoparticles due to it low concentration. The gas velocity in the shell side follows the Happel's free surface model.

The following assumptions were considered in the model development [27,29,30].

- The process is at steady-state and isothermal conditions since the fluid flow remains at constant temperature as the lab is air conditions (~24 ºC) and no reaction is taking place.
- The nanoparticles are considered homogeneous and uniformly distributed in the interface layer [27].
- The fluid flow is incompressible and Newtonian, concentration of CNT nanoparticle in water-based nanofluid is very low and hence the effect of the presence of few nanoparticles in the liquid phase is negligible.
- Gas-liquid equilibrium is estimated by Henry's law.

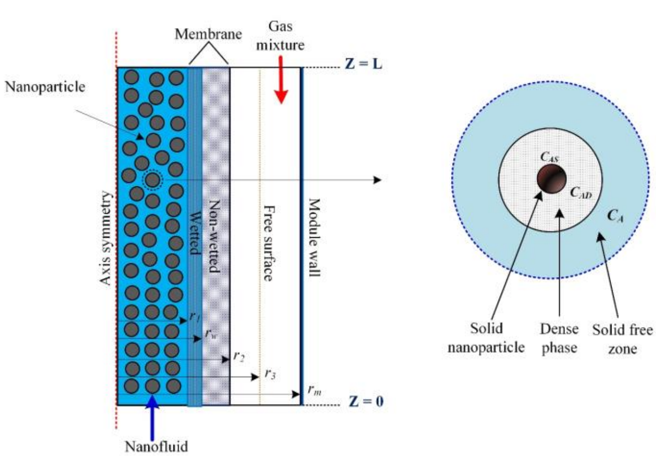

Fig. 2. (left) Schematic diagram of the axial cross-section of the membrane module showing partial wetting of the membrane and the flows of the nanofluid through the fiber tube side and gas through the shell side. (right) Diagram showing a solid nanoparticle and the surrounding phases and zones used in the model.

Based on Happel's free surface [34], the tubes are bounded by a laminar gas flow in the opposite direction to that of the liquid. At the Happel's hypothetical free surface of the fiber ($r = r_3$), symmetry is assumed. The steady state model assumed constant solvent properties, an ideal gas, and that the nanoparticles are spherical and homogeneous. The mathematical equations that describe the system behavior are developed for the tube side (solid and liquid phase), microporous membrane (wetted and non-wetted zones), and shell side. Accordingly, the continuity equations for CO_2 absorption are described in the following sections.

2.1. Tube Side: $(0 \le r \le r_1)$

The nanofluid contains nanoparticles suspended in a base fluid. In the model developed here, the nanoparticles are CNTs and the base fluid is water. The CNTs are black tubular nanostructures with an outer diameter of 8 nm, inner diameter of 2–5 nm, and length of 10 µm [26]. The nanofluid flowing in the lumen of the hollow fiber membranes removes CO_2 in the gas stream by absorption by the water and adsorption by the nanoparticles. The concentration of CO_2 in the solution free of solid particles (C_A) is written as follows:

$$\frac{D}{R^2}\left[\frac{\partial^2 C_A}{\partial \xi^2}+\frac{1}{\xi}\frac{\partial C_A}{\partial \xi}\right]+\frac{D}{L^2}\frac{\partial^2 C_A}{\partial \zeta^2}+\frac{u_{z_t}}{L}\frac{\partial C_A}{\partial \zeta}=0 \tag{1}$$

The concentration of CO_2 in the dense phase (C_{AD}) is:

$$\frac{D_n}{R^2}\left[\frac{\partial^2 C_{AD}}{\partial \xi^2}+\frac{1}{\xi}\frac{\partial C_{AD}}{\partial \xi}\right]+\frac{D_n}{L^2}\frac{\partial^2 C_{AD}}{\partial \zeta^2}+\frac{u_{z_t}}{L}\frac{\partial C_{AD}}{\partial \zeta}=R_d \tag{2}$$

The dimensionless parameters used in Eq. (1) and Eq. (2) are $\zeta = z/L$ and $\xi = r/r_3$, where D is the diffusion coefficient of CO_2 in the solid free zone and D_n is the diffusion coefficient of CO_2 in the dense solid phase. The diffusion coefficient of CO_2 in the dense phase liquid film around the nanoparticles can be written as follows [21]:

$$D_n = D\left(1 + 640 Re^{1.7} Sc^{\frac{1}{3}}\,\phi\right) \tag{3}$$

Here, ϕ is the solid volume fraction, and the Reynolds number, *Re*, of the nanoparticles under Brownian motion is:

$$Re = \left(\frac{18\,k\,T\rho}{\pi d_p \rho_p \mu^2}\right)^{0.5} \tag{4}$$

where k is Boltzmann's constant ($1.38\times10^{-23} J/K$), T is the temperature (K), ρ is the liquid density, d_p is the particle diameter, ρ_p is the particle density, and μ is the viscosity of the liquid. The Schmidt number Sc is written as:

$$Sc = \frac{\mu}{\rho D} \tag{5}$$

The adsorption rate R_d is written as:

$$R_d = k_p a_p (C_{AD} - C_{AS}) \tag{6}$$

where k_p is the solid–liquid mass transfer coefficient (m s^{-1}), a_p is the solid–liquid interfacial area (m^2 m^{-3}), C_{AD} is the solute concentration in the suspension (mol m^{-3}), and C_{AS} is the solute concentration at the interface of the particles (mol m^{-3}). The amount of CO_2 absorbed on the solid per unit mass of particles, q (mol kg^{-1}) can be given by:

$$\phi \rho_p \frac{v_{zt}}{L}\frac{\partial q}{\partial \xi} = k_p a_p (C_{AD} - C_{AS}) \tag{7}$$

The adsorption of the solute CO_2 on the particles is described by:

$$q = q_m \frac{k_d C_{AS}}{1 + k_d C_{AS}} \quad (8)$$

where, q_m is the highest quantity of adsorbed gas solute, and k_d ($m^3\ mol^{-1}$) is the adsorption coefficient of the solute. The velocity distribution in the tube side (v_{zt}) is assumed to follow Newtonian laminar flow.

$$v_{zt} = \frac{2Q_L}{\pi r_1^2 n_t}\left(1 - \left(\frac{r}{r_1}\right)^2\right) \quad (9)$$

The boundary conditions of the tube side are given as:

Solvent inlet side: $z = 0$ $\quad C_A = C_{AD} = 0$ (fresh solvent) (10)

Solvent exit side: $z = L$ $\quad \frac{\partial C_A}{\partial \xi} = \frac{\partial C_{AD}}{\partial \xi} = 0$ (convective flux) (11)

Tube center: $r = 0$ $\quad \frac{\partial C_A}{\partial \xi} = \frac{\partial C_{AD}}{\partial \xi} = 0$ (axial symmetry) (12)

Inner radius: $r = r_1$ $\quad C_A = C_{wm}$ (solubility of CO_2 in solvent) (13)

2.2. Skin layer of the hollow fiber membrane $r_1 \le r \le r_2$

2.2.1. Wetted section of membrane ($r_1 \le r \le r_w$)

The steady-state material balance for CO_2 transport, inside the wetted portion of the membrane is shown in Equation (14); there is no convection term as only diffusion is taking place in the wetted membrane.

$$\frac{D_{mw}}{R^2}\left[\frac{\partial^2 C_{wm}}{\partial \xi^2} + \frac{1}{\xi}\frac{\partial C_{wm}}{\partial \xi}\right] + \frac{D_{mw}}{L^2}\frac{\partial^2 C_{wm}}{\partial \zeta^2} = 0 \quad (14)$$

where C_{wm} is the CO_2 concentration in the wetted membrane section, and the diffusivity of CO_2 in the wetted membrane section is $D_{mw} = D_t \varepsilon/\tau$. The boundary conditions in this zone are given as:

Tube–wetted-membrane interface: $r = r_1$ $\quad C_{At} = C_{wm}$ (15)

Wet–dry membrane interface: $r = r_2$ $\quad C_{wm} = C_{Am} m$ (16)

Membrane inlet end: $z = 0$ $\quad \frac{\partial C_{wm}}{\partial z} = 0$ (17)

Membrane exit side $z = L$ $\quad \frac{\partial C_{wm}}{\partial z} = 0$ (18)

2.2.2. Non-wetting section of the membrane ($r_w \le r \le r_2$)

The steady state material balance for the transport of CO_2, inside the membrane (C_m), no convection term, only diffusion is taking place in membrane.

$$\frac{D_m}{R^2}\left[\frac{\partial^2 C_m}{\partial \xi^2} + \frac{1}{\xi}\frac{\partial C_m}{\partial \xi}\right] + \frac{D_m}{L^2}\frac{\partial^2 C_m}{\partial \zeta^2} = 0 \quad (19)$$

The boundary conditions are given as:

Interface of membrane-tube: $r = r_w$ $\quad C_m = C_{wm}/m$ (20)

Membrane-shell interface: $r = r_2$ $\quad C_A = C_{Ag}$ (21)

Dry membrane inlet end: $z = 0$ $\quad \frac{\partial C_m}{\partial z} = 0$ (22)

Dry membrane exit side: $z = L$ $\quad \frac{\partial C_m}{\partial z} = 0$ (23)

The diffusivity of CO_2 in the non-wetted membrane section, $D_m = D_g \varepsilon/\tau$. The material balance of the gas solute in the shell side at steady state (C_{Ag}) is:

$$\frac{D_g}{R^2}\left[\frac{\partial^2 C_{Ag}}{\partial \xi^2} + \frac{1}{\xi}\frac{\partial C_{Ag}}{\partial \xi}\right] + \frac{D_g}{L^2}\frac{\partial^2 C_{Ag}}{\partial \zeta^2} + \frac{v_{zs}}{L}\frac{\partial C_{Ag}}{\partial \zeta} = 0 \quad (24)$$

The boundary conditions:

Gas inlet side: $z = L$ $\quad C_{Ag} = C_{A0}$ (inlet concentration) (25)

Gas exit side: $z = 0$ $\quad \frac{\partial C_{Ag}}{\partial \xi} = 0$ (convective flux) (26)

Free surface: $r = r_3$ $\quad \frac{\partial C_{Ag}}{\partial \xi} = 0$ (symmetry) (27)

Shell-membrane interface: $r = r_2$ $\quad C_{Ag} = C_{Am}$ (28)

Assuming Happel's free surface model [34], the axial velocity in the shell side is expressed as

$$v_{zs} = \frac{2Q_g}{\pi\left(\frac{3r_3^4}{4} + \frac{r_2^4}{4} - r_2^2 r_3^2 - r_3^4 \ln\left(\frac{r_3}{r_2}\right)\right) nt}\left[r^2 - r_2^2 - 2r_3^2 \ln\left(\frac{r}{r_2}\right)\right] \quad (29)$$

Table 1 contains the parameters used in the simulation. The COMSOL Multiphysics 5.4 software package was used to solve the set of partial differential equations that described the separation process.

Table 1
Characteristics of the polypropylene membrane module and operating parameters used in the model.

Parameter	Values	Ref.
Inner fiber tube diameter (m)	0.32×10^{-3}	[26]
Outer fiber tube diameter (m)	0.45×10^{-3}	[26]
Inner module diameter(m)	2×10^{-2}	[26]
Module length (m)	40×10^{-2}	[26]
Total number of tubes	400	[26]
Membrane contact area (m^2)	0.16	[26]
CNT true density (g/cm^3)	2.2	[25]
CNT absorption capacity (mol/g)	1.57×10^{-2}	[26]
$D_{At}(m^2/s)$	$2.35\times10^{-6}e^{-\frac{2199}{T}}$	[35]
$D_{Ag}(m^2/s)$	1.855×10^{-6}	[36]
$D_{Am}(m^2/s)$	$D_{Ag}\varepsilon/\tau$	Calculated
$D_{solv}\ (m^2/s)$	$0.5D_{At}$	Calculated
$m=1/H$	$H=2.82\times10^{6}\exp\left(\frac{-2044}{T}\right)/RT$	[35]
Porosity, ε	0.50	[35]
Tortuosity, τ	$(2-\varepsilon)^2/\varepsilon$	[37]

3. Results and discussion

3.1. Model validation

The modeled surface plot of CO_2 concentration across the membrane module (tube, wet and dry membrane zones, and shell sides) is presented in Figure 3. An initial feed concentration of CO_2 of 0.5 mol.m^{-3} was selected to match the conditions used to generate experimental data [26] later used to validate the current mathematical model. The surface plot shows that the CO_2 concentration was much lower on the shell side than within the membrane and tube. This lower CO_2 concentration is attributed to absorption of the diffused CO_2 by the solvent. The arrows in Figure 3 represent the total CO_2 diffusion fluxes, where the smaller arrows in the membrane area are due to the slow diffusion flux through the membrane micropores.

The effect of inlet gas flow rate on the CO_2 removal rate along the gas–membrane interface is shown in Figure 4. The CO_2/N_2 gas mixture enters the membrane shell opposite to the solvent inlet port. The CO_2 is at its maximum initial feed concentration at the inlet port ($z = L$); hence, the removal rate is zero. As the gas mixture flows downward through the membrane shell side, CO_2 diffuses through the membrane to the nanofluid liquid solvent flowing in the lumen of the hollow fibers in the opposite direction, where the CO_2 is dissolved and consumed, resulting in a decrease in CO_2 concentration (increase in removal rate) as it travels through the shell side. The CO_2 removal rate decreases with increasing gas flow rate due to a reduction in the residence time of the gas inside the membrane module.

The model is validated with experimental data available in literature [26], as shown in Figure 5. The model predictions (solid lines) for both nanofluid (CNT + distilled water) and fresh water solvents are shown. The experimental data were in good agreement with the model predictions for cases with and without CNTs. As shown earlier, the CO_2 removal rate decreases with increasing inlet gas flow rate due to the reduced gas–liquid interaction time at higher gas flow rates. In addition, at higher flow rates of the gas and specific nanofluid flow rates, solvent saturation with the absorbed solute from the gas phase can occur.

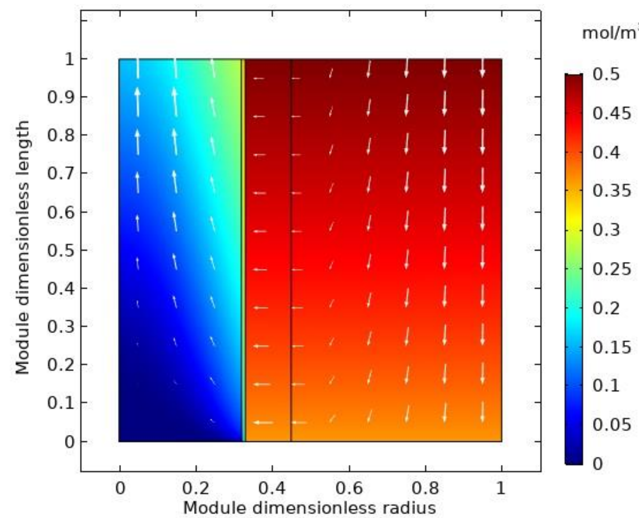

Fig. 3. Surface plot of CO_2 concentration in the tube, wetted membrane area (7%), dry membrane area, and shell section of HFMC ($CO_{2,o}$ = 0.5mol/m^3, Q_L=7 L/h, Q_g=16 L/h).

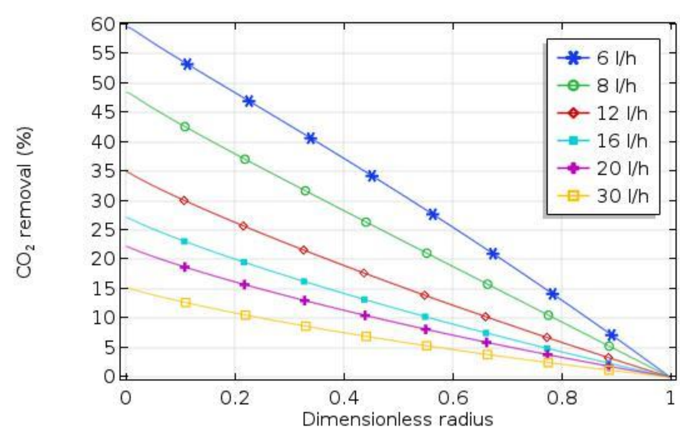

Fig. 4. Modeled CO_2 removal rate along the gas–membrane interface as a function of gas flow rate using 0.1 wt.% CNT (Q_L =7 L h^{-1}, $CO_{2,o}$ = 0.5 mol l^{-1}, T = 303 K, P = 0.3 bar).

The differences between the predicted results and the experimental data were quantified using the root mean square error (RMSE), as follows:

$$\mathrm{RMSE}=\left(\frac{\sum e_i^2}{n}\right)^{0.5} \quad (30)$$

where n is the sum of the investigated data points and e_i^2 is the square of the error between the predicted and experimental data point. The relative error (e_i) is as follows:

$$e_i=\frac{y_{exp}-y_{mod}}{y_{exp}} \quad (31)$$

where y_{exp} and y_{mod} are the experimental and predicted data points. The RMSE values of the distilled water and CNT/water systems were 0.074 and 0.057, respectively, indicating that the present model accurately predicts experimental membrane behavior. The results showed that, even though the CO_2 removal rate decreases with increasing gas flow rate, the mass transfer coefficient increases with increasing flow rate of the gas mixture [29].

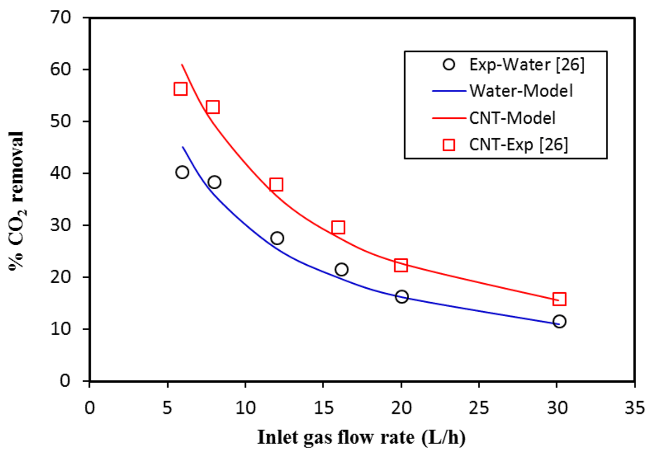

Fig. 5. Comparison of model prediction with available literature experimental data [26]. (0.1 w% CNT, $Q_L = 7$ L/h, $CO_{2,o} = 9900$ ppm, T=303 K, P = 0.3 bar).

Further comparison of the predicted results from the present model with those from another model that did not consider the wetting and dense phase resistance to mass transfer [29] showed that the results of the present model better matched the experimental data, as shown in Figure 6. This confirms that polypropylene polymeric membranes operate under partially wetted conditions when under the influence of pressure [31].

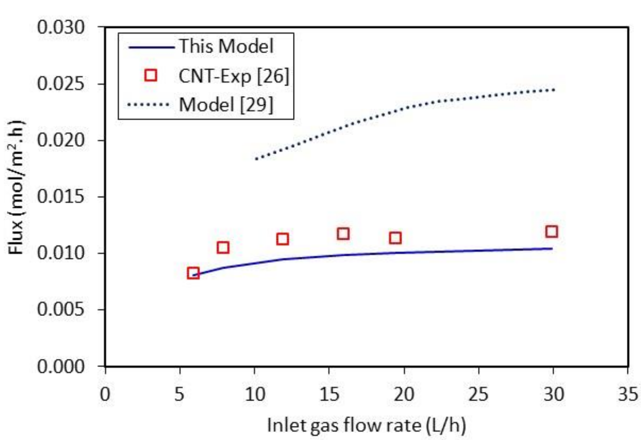

Fig .6. Comparison of the molar flux as a function of inlet gas flow rate calculated using the present model with that determined using a previous model [29] and experimental data with 0.1 wt.% CNT [26] ($\emptyset = 0.005$, $Q_L = 7$ L/h, $CO_{2,o} = 0.5$ mol/m^3).

Figure 7 shows that the enhancement factor as a function of inlet gas flow rate predicted by the present model agrees well with experimental data from the literature [26]. In addition, for a fixed nanoparticle concentration, the inlet gas flow rate did not significantly affect the enhancement factor; as the nanoparticles are saturated, increasing the flow rate does not result in further improvements. Similarly, the effect of nanoparticle volume fraction on the enhancement factor is shown in Figure 8 for the present predictions and the experimental data [26], where good agreement between the two was observed. The nanoparticle volume fraction did not significantly affect the enhancement factor. Although, increasing the nanoparticle concentration theoretically increases CO_2 removal, and hence the enhancement factor, increasing the nanoparticle concentration can also result in particle agglomeration on the membrane surface. This can block the membrane pores, resulting in a decrease in the gas–liquid interface area and lower removal rate. In addition, the nanoparticle concentration affects the stability of the nanofluid, which can reduce the absorption efficiency of the hollow fiber membrane contactor.

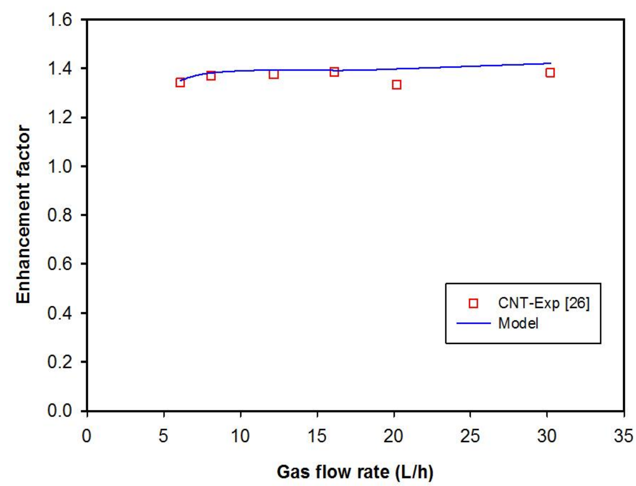

Fig. 7. Enhancement factor as a function of inlet gas flow rate, as predicted by the present model and determined experimentally [26] (0.1 wt.% CNT, $Q_L = 7$ L h^{-1}, 303 K).

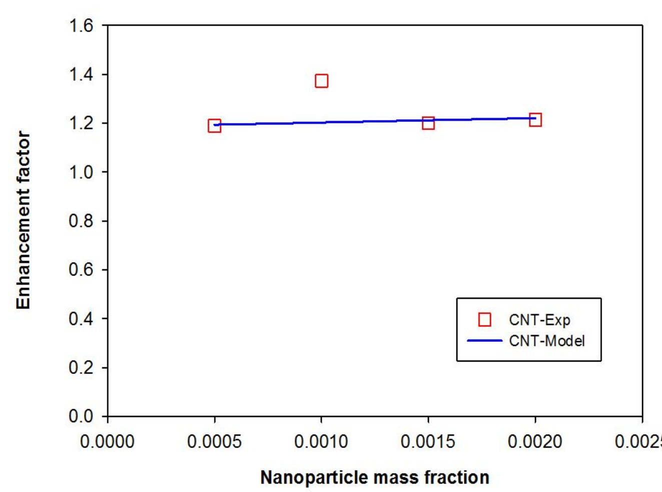

Fig. 8. Effect of nanoparticle mass fraction on the enhancement factor. Comparison of model predictions and experimental data [26] ($Q_L = 7$ L h^{-1}, $Q_g = 16$ L h^{-1}, 9000 ppm CO_2, T=303 K)

To further validate the model, we demonstrated that the effect of nanofluid flow rate on the CO_2 removal rate predicted by the model and determined experimentally [25] were in good agreement, as shown in Figure 9. The figure indicates that the CO_2 removal rate increases with increasing liquid flow rate, while the CO_2 deduction proficiency increases with increasing liquid flow rate due to a reduction in the thickness of the resistance mass transfer film [29].

The effect of the diameter of the solid nanoparticles on the CO_2 removal rate is shown in Figure 10. There is a sharp decrease in the CO_2 removal rate for particle sizes between 10 to 200 nm, while further increase in particle size did not significantly affect the removal rate. The decrease in the removal rate with increasing particle size is attributed to the lower liquid–solid interface area, as observed by Koronaki et al. [28].

The effect of inlet gas solute mole fraction on the CO_2 removal flux is shown in Figure 11, where it can be seen that the removal flux increases with increasing CO_2 concentration. This is attributed to the further CO_2 molecules diffusing toward the membrane for higher CO_2 concentrations. The more CO_2 absorbed, the higher the removal flux. This can be ascribed to an increase in the mass-transfer driving force. In contrast, there is only a slight effect of the inlet CO_2 mole fraction on the CO_2 removal rate, as shown in Figure 12. The figure shows that the model predictions and experimental data [26] agree well; hence, the model is suitable for studying parameters other than those experimentally investigated.

4. Conclusions

A compressive mathematical model was developed to represent the CO_2 absorption enhanced by aqueous CNT nanofluids considering the partially wetted mode of a hollow fiber membrane contactor system. The model divides the membrane absorption process into five zones, where the nanofluid in the tube side is modeled as a solid-free phase and dense phase where Brownian motion and grazing effects took place. The membrane side is divided into two zones; partially wetted and non-wetted segments. The shell side through which gas flows is considered as one zone. The present model predictions were in good agreement with experimental data reported in literature and showed better results than those of a similar model that did not consider the wetting and dense phase resistance to mass transfer. This model offers a viable method for exploring the mechanisms of CO_2 capture in the existence of nanoparticles, which is a promising method for enhancing CO_2 absorption and the performance of gas–liquid hollow fiber membrane contactors. The simulation results revealed that the liquid flow rate and CNT weight fraction in the nanofluid significant affect the CO_2 removal rate. For example, at an inlet gas flow rate of 20 l h^{-1}, around 20% CO_2 removal is achieved with 0.1 wt.% CNT, and approximately 45% of the CO_2 is removed using 0.25 wt.% CNT in a water-based nanofluid.

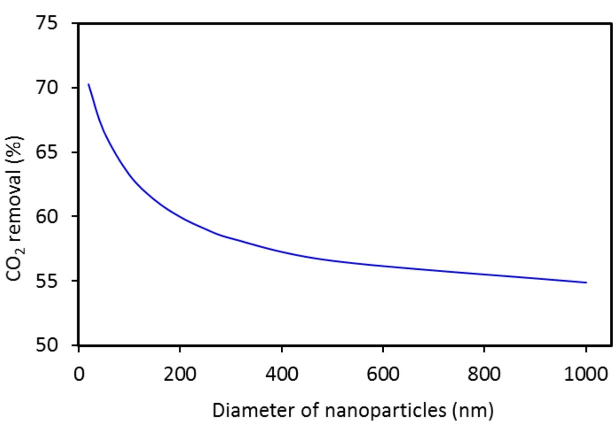

Fig. 9. Effect of liquid flow rate on CO_2 removal by CNT–water-based nanofluids (0.25 wt.% CNT, Inlet gas flow rate = 16 l h^{-1}, inlet concentration = 40%, T = 303 K).

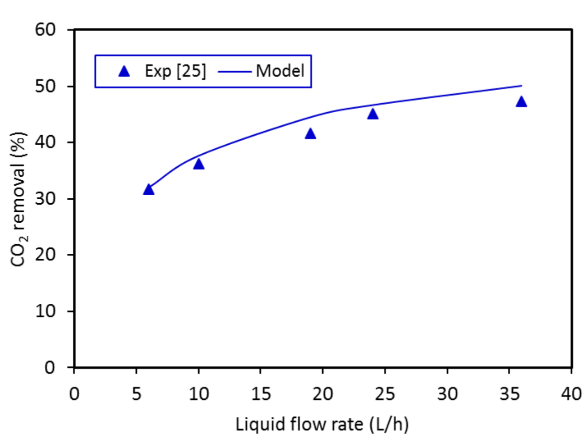

Fig. 10. Fraction of CO_2 removal as a function of nanoparticle diameter.

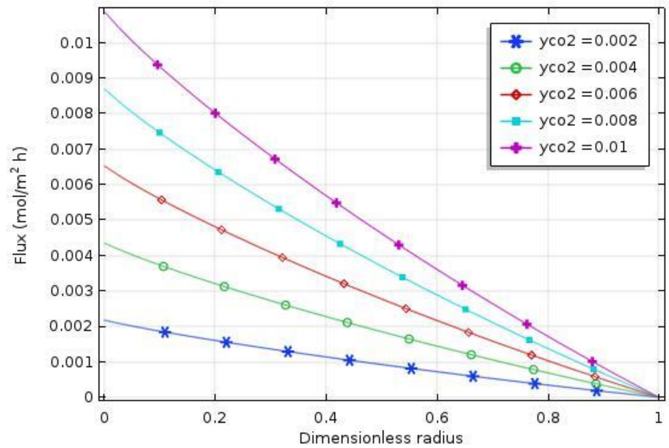

Fig. 11. Effect of inlet CO_2 mole fraction on the CO_2 removal flux $(Q_{liq} = 7\ L/h,\ Q_{gas} = 16\ L/h,\ T = 303\ K)$.

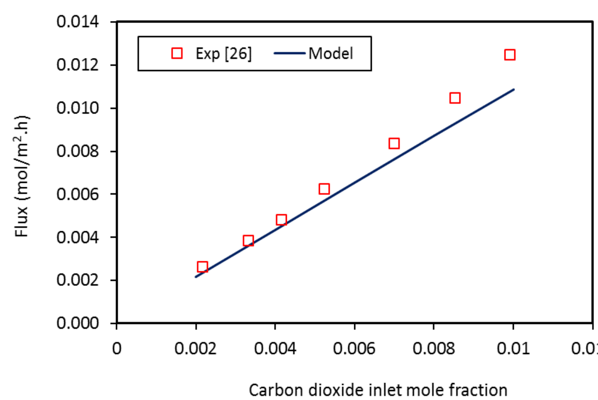

Fig. 12. Effect of CO_2 inlet mole fraction on the CO_2 removal flux $(Q_L = 7\ liter/h,\ Q_g = 16\ liter/h,\ T = 303\ K)$.

Acknowledgement

The author would like to acknowledge UAE University for the financial support (UPAR grant number: 31N374).

Nomenclature

A_T	Total membrane area, m^2
$C_{g,in}$	Inlet gas concentration, mol·m^{-3}
$C_{g,out}$	Outlet gas concentration, mol m^{-3}
C_i	Concentration of component i ; 1: CO_2, 2: N_2
$C_{i,m}$	Concentration of component i in the membrane section, mol m^{-3}
$C_{i,mw}$	Concentration of component i in the wetted membrane section, mol m^{-3}
$C_{i,s}$	Concentration of component i in the shell section, mol m^{-3}
$C_{i,t}$	Concentration of component i in the tube section, mol m^{-3}
$C_{L,in}$	Inlet liquid concentration, mol m^{-3}
$C_{L,out}$	Outlet liquid concentration, mol m^{-3}
$CO_{2,o}$	Inlet CO_2 concentration, mol m^{-3}

D_i	Diffusion coefficient of component i, m^2/s
D_{At}	Diffusivity of CO_2 in liquid solvent at the tube side, m^2/s
D_{Ag}	Diffusivity of CO_2 in gas phase at the shell side, m^2/s
D_{Am}	Diffusivity of CO_2 in membrane pores, m^2/s
D_{solv}	Diffusivity of CO_2 in solvent, m^2/s
d_i	Inner diameter of hollow fiber diameter, m
d_o	Outer diameter of hollow fiber diameter, m
H	Henry's constant
L	Length of hollow fiber membrane, m
m	Distribution factor
P	Pressure, Pa
q	Absorbed amount of solute, mol kg^{-1}
q_m	Maximum amount of adsorption by nanoparticles, mol kg^{-1}
Q_g	Inlet gas flow rate, m^3s^{-1}
Q_L	Inlet liquid flow rate, m^3s^{-1}
R	Universal gas constant, 8.314 J $mol^{-1}.K^{-1}$
r_1	Inner tube radius, m
r_2	Outer tube radius, m
r_3	Happel's free radius, m
r_w	Radius of wetted portion of membrane, m
T	Absolute temperature, K
μ	Viscosity of liquid, Pa s
v_z	Velocity of fluid inside the module in the z-direction, m s^{-1}
v_{zs}	Velocity of gas in the shell side, m s^{-1}
v_{zt}	Velocity of liquid in the tube side, m s^{-1}
$v_{z'avg}$	Average velocity, m s^{-1}
Z	Axial distance, m

Greek letters

ρ	Fluid density, kg m^{-3}
ρ_p	Solid particle density, kg m^{-3}
$\emptyset$	Nanoparticle volume fraction
ε	Membrane porosity
ξ	Dimensionless module radius, r/R
ζ	Dimensionless module length, z/L

References

[1] R. Wang, D. Li, D. Liang, Modeling of CO_2 capture by three typical amine solutions in hollow fiber membrane contactors. Chem. Eng. Process. Process Intensif. 43 (2004) 849-856.

[2] A. Gabelmana, S. Hwang, Hollow fiber membrane contactors, J. Membr. Sci. 159 (1999) 61-106.

[3] P. Luis, T.V. Gerven, B.V. der Bruggen, Recent developments in membrane-based technologies for CO_2 capture, Prog. Energy Combust. Sci. 38 (2012) 419-448.

[4] V. Dindore, D. Brilman, G. Versteeg, Modelling of cross-flow membrane contactors: mass transfer with chemical reactions, J. Membr. Sci. 255 (2005) 275-289.

[5] Z. Zhang, Y. Yan, L. Zhang, S. Ju, Numerical simulation and analysis of CO_2 removal in a polypropylene hollow fiber membrane contactor. Int. J. Chem. Eng. (2014) 256840.

[6] Z. Qi, E. Cussler, Microporous hollow fibers for gas absorption: I. Mass transfer in the liquid, J. Membr. Sci. 23 (1985) 321-332.

[7] Z.A. Tarsa, S.A.A. Hedayat, M. Rahbari-Sisakht, Fabrication and characterization of polyetherimide hollow fiber membrane contactor for carbon dioxide stripping from Monoethanolamine Solution, J. Membr. Sci. Res. 1 (2015) 118-123

[8] N.M. Ghasem, M. Al-Marzouqi, Modeling and experimental study of carbon dioxide Absorption in a Flat Sheet Membrane Contactor, J. Membr. Sci. Res. 3 (2017) 57-63

[9] N.M. Ghasem, M. Al-Marzouqi, L.P. Zhu, Preparation and properties of polyether sulfone hollow fiber membranes with o-xylene as additive used in membrane contactors for CO_2 absorption, Sep. Purif. Technol. 12 (2012) 1-10.

[10] N.M. Ghasem, M. H. Al-Marzouqi, A. Duaidar, Effect of quenching temperature on the performance of polyvinylidene fluoride microporous hollow fiber membranes fabricated via thermally induced phase separation technique on the removal of CO_2 from CO_2 - gas mixture, Int. J. Greenh. Gas Control 5 (2011) 1550–1558.

[11] A. Mansourizadeh, A.F. Ismail, A developed asymmetric PVDF hollow fiber membrane structure for CO_2 absorption, Int. J. Greenh. Gas Control 5 (2011) 374–380.

[12] A. Mansourizadeh, A.F. Ismail, M.S. Abdullah, B.C. Ng, Preparation of polyvinylidene fluoride hollow fiber membranes for CO_2 absorption using phase inversion promoter additives, J. Membr. Sci. 355 (2010) 200-207.

[13] C. Feng, R. Wang, H. Zhang, L. Shi, Diverse morphologies of PVDF hollow fiber membranes and their performance analysis as gas/liquid contactors, J. Appl. Polym. Sci. 119 (2011) 1259-1267.

[14] P. Sukitpaneenit, T.S. Chung, Molecular design of the morphology and pore size of PVDF hollow fiber membranes for ethanol-water separation employing the modified pore-flow concept, J. Membr. Sci. 374 (2011) 67-82.

[15] S. Atchariyawut, C. Feng, R. Wang, R. Jiraratananon, D.T. Liang, Effect of membrane structure on mass-transfer in the membrane gas–liquid contacting process using microporous PVDF hollow fibers, J. Membr. Sci. 285 (2006) 272–281.

[16] A. Mansourizadeh, A.F. Ismail, Hollow fiber gas–liquid membrane contactors for acid gas capture: a review, J. Hazard. Mater. 171 (2009) 38-53.

[17] J.-K. Kim, J.Y. Jung, Y.T. Kang, Absorption performance enhancement by nano-particles and chemical surfactants in binary nanofluids, Int. J. Refrig. 30 (2007) 50-57.

[18] S.M.H.H. Amrei, S. Memardoost, A.M. Dehkordi, Comprehensive modeling and CFD simulation of absorption of CO_2 and H_2S by MEA solution in hollow fiber membrane reactors, AIChE J. 60 (2014) 657-672

[19] D. Wen, Y. Ding, Experimental investigation into convective heat transfer of nanofluids at the entrance region under laminar flow conditions, Int. J. Heat Mass Trans. 47 (2004) 5181-5188

[20] S. Chol, Enhancing thermal conductivity of fluids with nanoparticles ASME-Publications-Fed, 231 (1995) 99-106.

[21] E. Nagy, T. Feczkó, B. Koroknai, Enhancement of oxygen mass transfer rate in the presence of nano sized particles, Chem. Eng. Sci. 62 (2007) 7391-7398

[22] B. Rahmatmand, P. Keshavarz, S. Ayatollahi, Study of absorption enhancement of CO_2 by SiO_2, Al_2O_3, CNT, and Fe_3O_4 Nanoparticles in water and amine solutions, J. Chem. Eng. Data 61 (2016) 1378-1387.

[23] S.H. Esmaeili-Faraj, M. Nasr Esfahany, Absorption of hydrogen sulfide and carbon dioxide in water based nanofluids, Ind. Eng. Chem. Res. 55 (2016) 4682-4690.

[24] I.T. Pineda, J.W. Lee, I.K. Jung, T. Yong, CO_2 absorption enhancement by methanol-based Al_2O_3 and SiO_2 nanofluids in a tray column absorber. Int. J. Refrig. 35 (2013) 1402-1409.

[25] A. Golkhar, P. Keshavarz, D. Mowla, Investigation of CO_2 removal by silica and CNT nanofluids in microporous hollow fiber membrane contactors, J. Membr. Sci. 433 (2013) 17-24.

[26] A. Peyravi, P. Keshavarz, D. Mowla, Experimental investigation on the absorption enhancement of CO2 by various nanofluids in hollow fiber membrane contactors, Energy Fuel., 29 (2015) 8135-8142

[27] L. Sumin, X. Min, S. Yan, D. Xiangjun, Experimental and theoretical studies of CO_2 absorption enhancement by nano-Al_2O_3 and carbon nanotube particles, Chin. J. Chem. Eng. 21, 21 (2013) 983–990.

[28] I.P. Koronaki, M.T. Nitsas, Ch.A. Vallianos, Enhancement of carbon dioxide absorption using carbon nanotubes – A numerical approach, Appl. Thermal Eng. 99 (2016) 1246-253.

[29] M. Darabi, M. Rahimi, and A.M. Dehkordi, Gas absorption enhancement in hollow fiber membrane contactor using nanofluids: Modeling and Simulation, Chem. Eng. Process. Process Intensif. 119 (2017) 7-15.

[30] M. Rezakazemi, M. Darabi, E. Soroush, M. Mesbah, CO_2 absorption enhancement by water-based nanofluids of CNT and SiO_2 using hollow-fiber membrane contactor, Sep. Purif. Technol. 210 (2019) 920-926.

[31] H. Mohammaddoost, A. Azari, M. Ansarpour, S. Osfouri, Experimental investigation of CO_2 removal from N_2 by metal oxide nanofluids in a hollow fiber membrane contactor, Int. J. Greenh. Gas Control 69 (2018) 60–71.

[32] M. Hossein K. Darvanjooghi, M. Esfahany, S. Esmaeili-Faraj, Investigation of the effects of nanoparticle size on CO_2 absorption by silica-water nanofluid, Sep. Purif. Technol. 195 (2018) 208–215

[33] Y. Lv, X. Yua, S.-T. Tua, J. Yanb, E. Dahlquist, Wetting of polypropylene hollow fiber membrane contactors, J. Membr. Sci. 362 (2010) 444–452.

[34] J. Happel, Viscous flow relative to arrays of cylinders, AIChE J. 5 (1959) 174–177.

[35] G.F. Versteeg, W. Van Swaalj, Solubility and diffusivity of acid gases (carbon dioxide, nitrous oxide) in aqueous alkanolamines solutions, J. Chem. Eng. Data 33 (1988) 29–34.

[36] E.L. Cussler, Diffusion: Mass transfer in fluid systems, Cambridge University Press, 2009.

[37] S.B. Iversen, V.K. Bhatia, K. Dam-Johansen, G. Jonsson, Characterization of microporous membranes for use in membrane contactors, J. Membr. Sci. 130 (1997) 205-217.

[38] L. Kucka, E.Y. Kenig, A. Gorak, Kinetics of gas–liquid reaction between carbon dioxide and hydroxide ions, Ind. Eng. Chem. Res. 41 (2002) 5952–5957.